Creating Superhydrophobic Surface Structures *Via* the Rose Petal Effect on Stainless steel with a Picosecond Laser

J. LAWRENCE* AND D.G. WAUGH

School of Mechanical, Aerospace and Automotive Engineering
Faculty of Engineering, Environment and Computing
Coventry University
Gulson Road
Coventry
CV1 2JH

*Corresponding author:

J. Lawrence
School of Mechanical, Aerospace and Automotive Engineering
Faculty of Engineering Environment and Computing
Coventry University
Gulson Road
Coventry
CV1 2JH
Email: jonathan.lawrence@coventry.ac.uk
Tel: +44 (0) 24 7765 7688

ABSTRACT

A sub-five picosecond laser was used to create a range of surface structures on stainless steel. The stainless steel exhibited a transition in surface from laser-induced periodic surface structures (LIPSS), of the order of 1 µm, to grains *via* a LIPSS/mountainous double structure. The wettability of the stainless steel surface was characterized by measuring the contact angle and was observed to have changed from a hydrophilic surface (63.6°) to a superhydrophobic one (160.0°) due to the laser processing. This equated to an increase in contact angle of approximately 100.0°. This has been attributed to the creation of hierarchical surface structures that exhibit the rose petal effect. Additionally the contact angle hysteresis and the surface roughness have been measured and characterized. The use of a picosecond laser to generate such surfaces demonstrates a viable, low-cost alternative to using a femtosecond laser.

Keywords: Picosecond laser, stainless steel, laser induced periodic surface structures (LIPSS), wettability, contact angle, superhydrophobicity; rose petal effect, wetting regime transition

1 INTRODUCTION

Superhydrophobic surfaces are already a large, and expanding, area of study within the field of wettability and adhesion. For a material to be deemed superhydrophobic it primarily must produce a contact angle ≥150.0° [1]. Superhydrophobicity exists in nature through two common mechanisms, the lotus effect and the rose petal effect. Both types of superhydrophobicity exhibiting are hierarchical in composition; that is, combining nanostructuring on top of microstructuring. The Lotus effect is an example of a self-cleaning surface where there is very low adhesion between the droplet and the surface allowing for easy run-off with any dust particles being collected along the way. The level of contact angle hysteresis in this case will be very low as the surface actively repulses the droplet [2]. This is theorized to be caused by air filling the gaps within the nano- and microstructure providing a continuous surface formed of both air and the material that the droplet rests on. The texturing of the surface causes the superhydrophobicity, with the heterogeneity of the surface causing very low adhesion [3].

Alternatively, the rose petal effect has a very high level of adhesion between the surface and the droplet, leading it to being described as pseudo-superhydrophobic in some respects due to the low roll off of droplets. This is despite maintaining very low levels of contact between the droplet and the surface [2]. Whilst this appears counter-intuitive that a surface may have a low contact angle but high adherence to a liquid, it is caused by differences in the microstructure leading to higher hysteresis values (high hysteresis being indicative of stronger adhesion). Rose petal-like surfaces typically have larger surface features which allow the liquid to impregnate into some of the surface structures whilst the air-trapping maintains in others. This extra level of wetting provides the adhesive force [3, 4]. Obviously there is a limit to the adhesive strength of these surfaces, with sufficiently large droplets exhibiting roll off. The Lotus effect obeys a Cassie-Baxter type wetting regime. The other major wetting regime, the Wenzel regime, differs from the Cassie-Baxter regime with the droplet being impregnated into any surface texture. The rose petal effect is somewhere in-between the two, with air pockets and water impregnation occurring in different parts of the

surface. This ‘mixed-state’ wetting regime has been described as the Cassie-impregnating wetting regime [3, 4].

The ability of laser beams to modify the surfaces of most material types including polymers, semiconductors, glasses, metals, ceramics and woods has been amply demonstrated [5-10]. Key to the flexibility of laser processing is the ability to match the wavelength of the emitted light to the absorption bands of the material being processed to ensure the beam couples into the surface. The use of ultrashort pulses in the pico- and femtosecond regime has led to the development of laser-induced periodic surface structures (LIPSS), which have been suggested for application in medical technologies due to their adhesive properties [11]. LIPSS can form when a surface is struck by ultrashort, low energy, high frequency pulses. These generate periodic structures that are typically of the order of the excitation wavelength in size [12]. Whilst femtosecond lasers are considered superior for structuring surfaces, it should be noted that picosecond lasers are a more established technology towards industrialization, and are considerably lower in cost. This paper demonstrates the production of a range surface structures on stainless steel, several of which demonstrate the rose-petal effect.

2 APPARATUS AND EXPERIMENTAL PROCEDURES

A series of 64 4 × 4 mm^2 samples were laser machined into a 50 × 50 mm^2 stainless steel plate (Goodfellow, Ltd.) using a picosecond pulse laser (HE-1060-10uJ-SP; Fianium, Ltd.) with a galvanometric scanning head. Each sample was processed in a series of rastered lines. Prior to processing, the stainless steel was cleaned with isopropyl alcohol in an ultrasonic bath for three minutes. After cleaning, the sample was dried in an oven for two hours. The pulse power was maintained at 10 µJ and the pulse frequency at 500 kHz, yielding an output power of 5 W. The laser had a spot size of approximately 20 to 25 µm, an emission wavelength of 1064 nm and a maximum pulse duration of 5 ps. A summary of the processing parameters tested can be found in Table 1.

Microstructure was assessed using a benchtop scanning electron microscope (SEM) (TM3030; Hitachi Corporation). Roughness measurements were made using a three-dimensional (3-D) chromatic confocal imager (Micromersure2; STIL SA) and wettability measurements were taken with goniometer (OCA20; Dataphysics, GmbH). Wettability measurements were taken >1 month after the laser processing to ensure any hydrophobic recovery was accounted for. Whilst contact angles are typically stable after two to three

weeks, most research in this regard has been done on polymers rather than metals; consequently, extra time was allotted in accordance with the work of Guckenberger *et al* [13]. The samples were re-cleaned to ensure dust removal using the same method as that used prior to laser processing. Advancing and receding contact angle measurements were taken using the sessile drop needle-in method allowing for the calculation of hysteresis.

3 RESULTS AND DISCUSSION

Figure 1 shows selected examples of the surface structure types generated by the picosecond laser pulses. The most common form of LIPSS seen in the literature are low spatial frequency surface structures which have a periodicity roughly equal to that of the laser wavelength. These type of LIPSS structures are visible in Figures 1(a) to (c), where the periodicity was around 1 μm which matches with the wavelength of the laser. There were no real changes in the way the surface is structured with diminishing scan spacing at these high processing speeds.

Slowing the scanning speed results in the formation of a double structure of low spatial frequency LIPSS separated by a larger, mountainous, structure of elevated stainless steel combined with micropits (see Figures 1(d) to (f)). The LIPSS appeared to have formed in what could be described as the heat affected zone (HAZ); that is, the less energy intensive part of the Gaussian beam distribution of the laser pulse, with the mountainous structure forming under the more energy intensive centre of the beam. At this level of processing speed, reducing the spacing decreases the proportion of LIPSS visible, which coincides with each successive scan processing over previously generated LIPSS structures.

At the slowest scanning speed the surface had significantly changed (see Figure 1(g) and Figure 1(i). Figure 1(g) shows large melted mountainous regions separated by cracking and the appearance of some small grains. Reducing the spacing led to the appearance of a small grain-type structure all over the surface (see Figure 1(h)), which turned into a larger grain-like structure in Figure 1(i). Figure 1(i) shows Sample 7h which had a very narrow line spacing coupled with a very slow scan speed. This combination caused intensive processing of the stainless steel, with the separation of each line scan being considerably smaller than the spot size of the laser resulting in successive re-structuring of the stainless steel. It can be seen that the once comparatively featureless surface of the stainless steel (shown in Figure 1(AR) had been fractured into a relatively ordered granular structure. The majority of grains appeared to range between 10 and 20 μm in diameter. Each of these surfaces (Figure 1(g) and

Figure 1(i)) exhibited the appearance of a fine nanostructure on the surface of the larger features. These structures could be classed as hierarchical in nature due to this combination of micro- and nanostructuring [14]. The surfaces shown in Figures 1(a) to (c) were consistently microstructured, whilst the surfaces in Figures 1(d) to (f) show a combination of structure sizes on the surface. These structures, particularly for Figure 1(d) and Figure 1(e), were rarely combined one on top of the other, as in Figure 1(g) and Figure (i), and so cannot be truly called hierarchical; however, Figure 1(f) did start to appear hierarchical. Describing the entirety of the processed samples, as the rows progress the LIPSS structures of Row A transform into the double structures seen in Row D through the appearance of stripes that became the mountains and are more visible at lower spacings. Progressing towards Row H one sees the LIPSS structures disappear completely and the mountainous structure slowly transforms *via* cracking into the granular surface. At the most intense levels of processing (Sample 7h and Sample 8h) complete destruction of the surface was observed with no discernible structures visible, presumably due to increased debris levels limiting the ability to focus the SEM.

Figure 2(a) and Figure 2(b) demonstrate the change in wettability from as-received stainless steel to the most hydrophobic laser processed surface. The change in average advancing contact angle displayed was 63.6 to 160.0° and in average receding contact angle 51.4 to 153.9°. In each case the increase in contact angle caused by laser processing was approximately 100.0° turning the surface from hydrophilic to superhydrophobic. Figure 2(c) summarizes a selection of the advancing and receding contact angles of the laser processed stainless steel samples as well as showing the transition from hydrophilic-hydrophobic-superhydrophobic states. Of those selected, Samples 1h, 4h and 7d exhibited superhydrophobicity, a dramatic change from the hydrophilic as-received surface. All laser processed samples displayed contact angles of at least 100.0°. Relating the contact angle change to the surface structure, both LIPSS and granular structures were hydrophobic in nature; however, LIPSS-only and ordered grain structures do not produce superhydrophobicity. The transition from the double structure to the granular structure provides the optimum window for superhydrophobicity to occur. This further supports the observations that these structures are hierarchical.

To determine the type of superhydrophobic surface, and thus the wetting regime, a simple test was performed. This was achieved by placing a droplet sufficiently small that its surface tension can overcome any influence from its weight and gravity, in this case 5 µl of H_2O, on the surface of the processed stainless steel and inverting it. If the droplet runs off

easily then the Lotus effect is dominant. If the droplet stays attached to the surface then the Rose petal effect dominated due to the strong adhesion force caused by the Cassie-impregnating wetting regime [15]. The result of this test can be seen in Figure 2(d), clearly demonstrating the rose petal effect. The increase in hydrophobicity can be attributed initially to, generation of a consistent microstructure (LIPSS). The transitional structure of LIPSS and mountainous peaks that combined different feature sizes increased the level of hydrophobicity further, approaching superhydrophobic levels. As the level of processing increased further, true hierarchical surfaces formed with superhydrophobic levels of wetting peaking with Sample 1h. The contact angle then began to decrease as the grains formed on the surface. This can be attributed to the formation of larger microchannels, likely at the grain boundaries, which acted to channel more of the fluid away; that is, these structures are less effective at air trapping. This would increase the level of impregnation in the mixed state Cassie-impregnation regime and explains the lower contact angles seen in Sample 7h [16].

Analysis of the hysteresis of the laser processed samples, summarized in Table 2, elucidates further the wetting regime present. Of the two types of superhydrophobic surface, the lotus effect exhibits incredibly low levels of hysteresis (typically around 3.0°) that stay consistent as the drop size decreased. The Rose petal effect exhibited higher values of hysteresis that can change dramatically with increasing droplet size as other forces act to overcome the adhesive force [3]. The hysteresis values are suggestive of a rose petal type effect supporting the observations of the SEM and goniometry.

Surface roughness measurements (see Figure 3) of the stainless steel demonstrated an increase in mean roughness (S_a) post-laser processing. The slower the processing speed and thus the more processing that occurs, the rougher the eventual surface for equivalent scan spacing. It can be seen that the closer to the granular structure the rougher the surface, albeit that a fully granular structure is less rough than the transitional structures. There appeared to be no consistent trend between average roughness and the level of wetting as measured; however, resolution limitations of optical techniques may have been a factor and other measurements of roughness may be more suitable than S_a. These measurements suggest that the type of surface structure itself is more significant than average roughness in determining the eventual level of wetting which correlates with well with the literature [17, 18].

4 CONCLUSIONS

A process whereby a range of different surface structures have been generated in stainless steel using picosecond laser pulses has been demonstrated. Analysis of the surface showed the formation of laser-induced periodic surface structures (LIPSS) at high scan speeds, which transitioned towards a grain structure at very slow scan speeds. Contact angle goniometry demonstrated, with H_2O as the liquid, superhydrophobicity on some of the surfaces with a peak contact angle over 160.0°. This was a dramatic increase of close to 100.0° demonstrating a large, laser induced, transition in the surface from a hydrophilic state to a superhydrophobic one. Microscopic analysis showed the presence of hierarchical surface structures for the samples that exhibited superhydrophobicity. The laser processed stainless steel also exhibited high levels of adhesion between the droplet and the surface allowing identification of the presence of the rose petal effect and thus the mixed state Cassie-impregnating wetting regime. This was supported by examination of the level of hysteresis. Knowledge of the hysteresis, hierarchical surface and the long-term stability of the laser generated surfaces yields better control of the superhydrophobicity.

ACKNOWLEDGEMENTS

The authors would like to acknowledge the valuable support of Giordano Menci and his supervisor, Prof. Barbara Previtali, of the Department of Engineering, Politecnico di Milano, Milan, Italy.

REFERENCES

[1] Wang S. and Jiang L. Definition of superhydrophobic states. *Advanced Materials* **19**(21) (2007), 3423-3424.

[2] Bormashenko E. Physics of solid–liquid interfaces: From the Young equation to the superhydrophobicity (Review Article). *Low Temperature Physics* **42**(8) (2016), 622-635.

[3] Bhushan B.and Nosonovsky M. The rose petal effect and the modes of superhydrophobicity. *Philosophical Transactions of the Royal Society A - Mathematical Physical and Engineering Sciences* **368**(1929) (2010), 4713-4728.

[4] Bormashenko E. and Starov V. Impact of surface forces on wetting of hierarchical surfaces and contact angle hysteresis. *Colloid and Polymer Science* **291**(2) (2013), 343-346.

[5] Waugh D.G., Lawrence J., Morgan D.J. and Thomas C.L. Interaction of CO_2 laser-modified nylon with osteoblast cells in relation to wettability. *Materials Science & Engineering C - Materials for Biological Applications* **29**(8) (2009), 2514-2524.

[6] Kontermann S., Gimpel T., Baumann A.L., Guenther K.M. and Schade W. Laser processed black silicon for photovoltaic applications. *Proceedings of the 2nd International Conference on Crystalline Silicon Photovoltaics (SiliconPV 2012).* 3-5 April 2012, Austin, TX., USA. **27**, pp. 390-395.

[7] Hodgson S.D., Waugh D.G., Gillett A. and Lawrence J. High speed CO_2 laser surface modification of iron/cobalt co-doped boroaluminosilicate glass and the impact on surface roughness, gloss and wettability. *Laser Physics Letters* **13**(7) (2016), 076102.

[8] Kubovsky I. and Babiak M. Color changes induced by CO_2 laser irradiation of wood surface. *Wood Research* **54**(3) (2009), 61-66.

[9] Shukla P.P., Swanson P.T. and Page C.J. Laser shock peening and mechanical shot peening processes applicable for the surface treatment of technical grade ceramics: A review. *Proceedings of the Institution of Mechanical Engineers Part B - Journal of Engineering Manufacture* **228**(5) (2014), 639-652.

[10] Hao L. and Lawrence J. Wettability modification and the subsequent manipulation of protein adsorption on a Ti6Al4V alloy by means of CO_2 laser surface treatment. *Journal of Materials Science: Materials in Medicine* **18**(5) (2007), 807-817.

[11] Weber J. and Holman T. Applications of LIPSS in polymer medical devices. *Official Gazette of the United States Patent and Trademark Office Patents.* 8th October 8 2013.

[12] Preusch F., Rung S. and Hellmann R. Influence of polishing orientation on the generation of LIPSS on stainless stainless steel. *Journal of Laser Micro Nanoengineering* **11**(1) (2016), 137-142.

[13] Guckenberger D.J., Berthier E., Young E.W.K. and Beebe D.J. Induced hydrophobic recovery of oxygen plasma-treated surfaces. *Lab on a Chip* **12**(13) (2012), 2317-2321.

[14] Gedvilas M., Miksys J. and Raciukaitis G. Flexible periodical micro- and nano-structuring of a stainless stainless steel surface using dual-wavelength double-pulse picosecond laser irradiation. *RSC Advances* **5**(92) (2015), 75075-75080.

[15] Sun J.S. and Wang J.G. Fabrication of superhydrophobic surfaces on FRP composites: from rose petal effect to lotus effect. *Journal of Coatings Technology and Research* **12**(6) (2015), 1023-1030.

[16] Bico J., Thiele U. and Quere D. Wetting of textured surfaces. *Colloids and Surfaces A - Physicochemical and Engineering Aspects* **206**(1-3) (2002), 41-46.

[17] Moon H.W., Yoon Y.J., Park J.H., Myung B-S. and Kim D.E. Dynamic wetting and boiling characteristics on micro-structured and micro/nano hierarchically structured surfaces. *Experimental Thermal and Fluid Science* **74** (2016), 19-26.

[18] Nosonovsky M. and Bhushan B. Hierarchical roughness makes superhydrophobic states stable. *Microelectronic Engineering* **84**(3) (2007), 382-386.

Column	Spacing (µm)	Row	Speed (mm/s)
1	30	A	500
2	26	B	300
3	22	C	150
4	18	D	80
5	14	E	40
6	10	F	20
7	6	G	10
8	2	H	5

TABLE 1

Picosecond laser operating parameters used in each of the 64 samples.

Sample	Hysteresis (°)
AR	12.3
1a	0.1
1d	14.4
1h	6.2
4a	5.7
4d	4.1
4h	5.9
7a	8.3
7d	7.2
7h	3.9

TABLE 2

Contact angle hysteresis for the as-received stainless steel and a selection of the picosecond laser processed stainless steel samples.

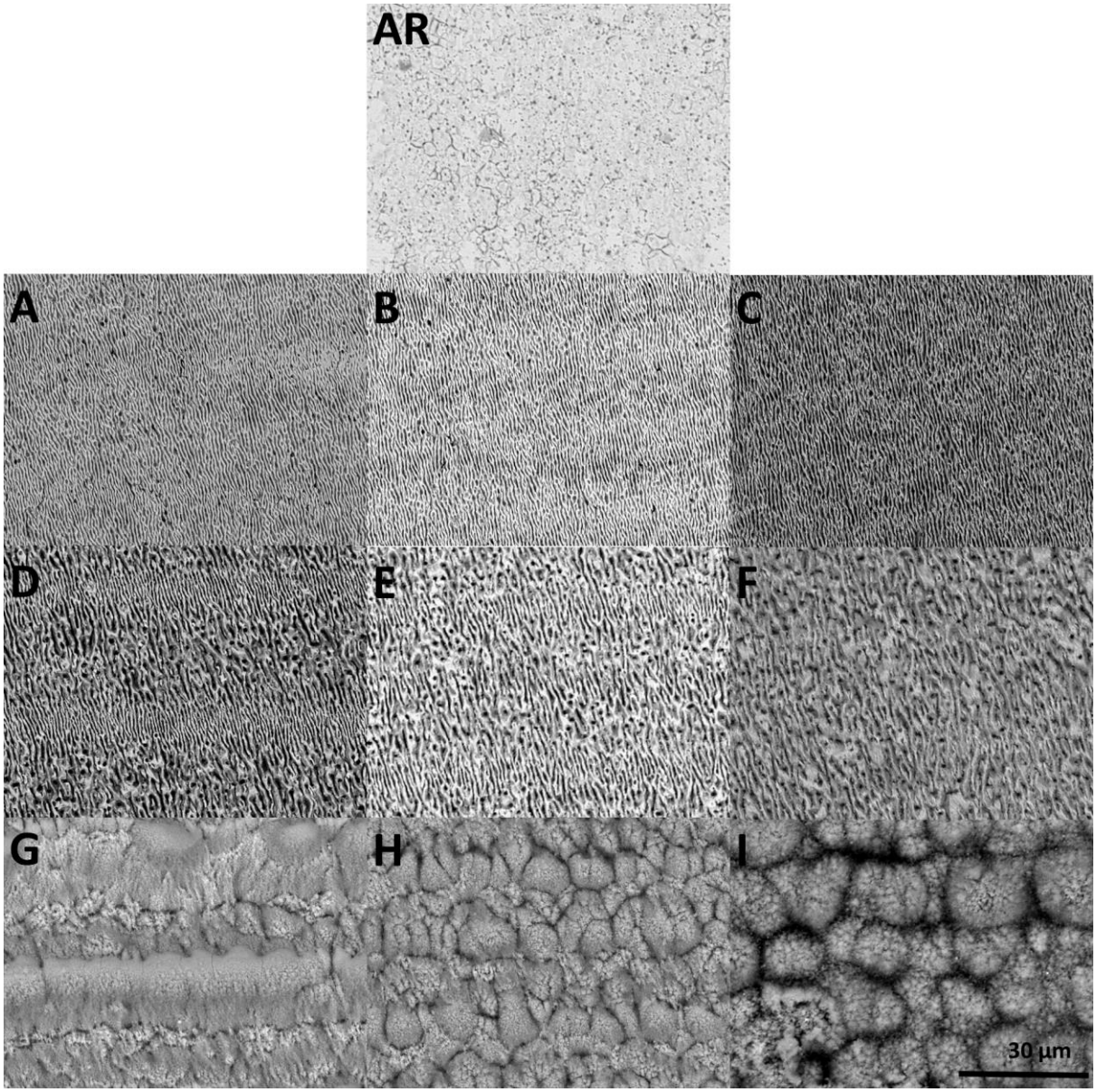

FIGURE 1

SEM micrographs of the as-received stainless steel (AR) and a selection of the laser modified surfaces: (a) Sample 1a; (b) Sample 4a; (c) Sample 7a; (d) Sample 1d; (e) Sample 4d; (f) Sample 7d; (g) Sample 1h; (h) Sample 4h; and (i) Sample 7h.

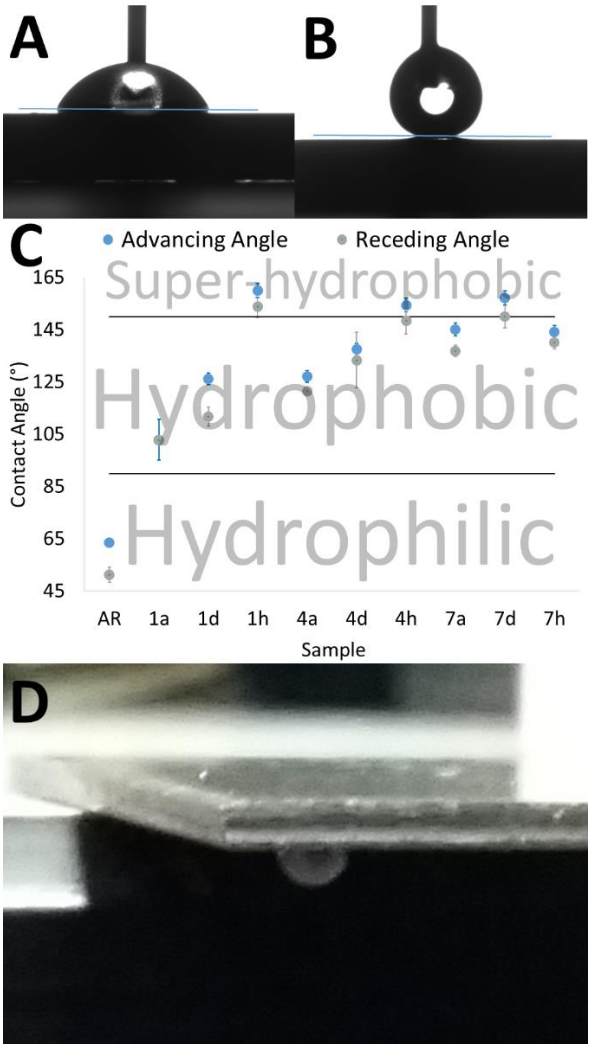

FIGURE 2

Goniometer images of water droplets on the surface of (a) the as-received stainless steel and (b) the picosecond laser processed stainless steel (the lines drawn on show the position of the surface at droplet); (c) graph showing the advancing and receding contact angles of the as-received and a selection of the picosecond laser processed stainless steel samples; and (d) an image of a 5 µl water droplet on inverted picosecond laser processed stainless steel demonstrating the rose petal effect [15].

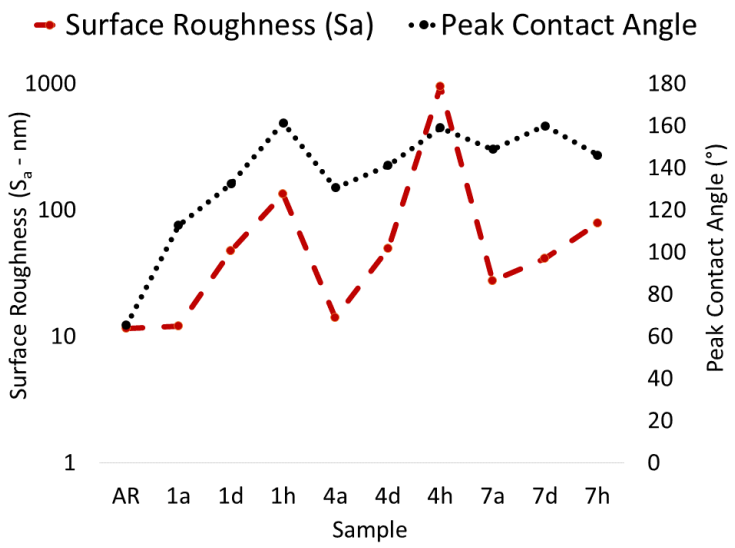

FIGURE 3

Graph of surface roughness (S_a) (plotted on a log scale) with contact angle for selected samples.